

# Improvement of an Extreme Heavy Rainfall Simulation Using Nudging Assimilation

Taichen FENG<sup>1</sup>, Zhiyuan HU<sup>2</sup>, Shankai TANG<sup>1</sup>, and Jianping HUANG<sup>1\*</sup>

<sup>1</sup> Key Laboratory for Semi-Arid Climate Change of the Ministry of Education, College of Atmospheric Sciences, Lanzhou University, Lanzhou 730000

<sup>2</sup> School of Atmospheric Sciences, Sun Yat-sen University, and Key Laboratory of Tropical Atmosphere–Ocean System of Ministry of Education, Zhuhai 519082

(Received June 8, 2020; in final form January 18, 2021)

## ABSTRACT

From 21 to 22 July 2012, Beijing and its surrounding areas suffered from an extreme precipitation event that was unprecedented relative to the past 61 years, and the event caused 79 deaths and reported direct economic losses of 11.64 billion Yuan. However, current models have difficulty to simulate the spatial and temporal distribution characteristics of such events. Therefore, improved simulations of these extreme precipitation processes are needed. In this study, nudging methods, including grid nudging (GN) and spectral nudging (SN), and more accurate surface type data retrieved from remote sensing were used in the Weather Research and Forecasting (WRF) model to simulate this extreme precipitation case. When the default city underlay surface of the WRF model was replaced by a more accurate urban surface (NU), the precipitation intensity could be better simulated, but the peak moment of precipitation seriously lagged. Although the peak precipitation intensity simulated by the GN experiment was weak, the simulated precipitation time was basically consistent with the observations. Using GN in only the outside domain could better simulate precipitation peaks, while using GN in both the inside and outside domains could better simulate the spatial distribution characteristics of precipitation. Additionally, the precipitation from GN could be better simulated than that from SN. Overall, the two nudging methods could contribute to better simulations of this case because the nudging methods could improve the simulations of 500-hPa geopotential height, 850-hPa water vapor transport, and low-level weather systems, which are the key factors in adjusting the spatial and temporal distributions of precipitation. This study is the basis for the investigation of the mechanism and attribution of extreme precipitation processes, and the results are of great significance for promoting understanding of and mitigating disasters caused by extreme precipitation.

**Key words:** extreme heavy precipitation, grid nudging (GN), Weather Research and Forecasting (WRF) model

**Citation:** Feng, T. C., Z. Y. Hu, S. K. Tang, et al., 2021: Improvement of an extreme heavy rainfall simulation using nudging assimilation. *J. Meteor. Res.*, **35**(2), 313–328, doi: 10.1007/s13351-021-0099-x.

## 1. Introduction

Extreme precipitation events have occurred frequently in recent decades; the increased frequency of these events globally has been due to a large increase in atmospheric water vapor and changes in the hydrological cycle under global warming (Kharin et al., 2007; Paul and Tapio, 2009). These events could induce natural disasters, e.g., flooding and landslides, and then affect human societies (Ding, 1994). In China, the trend of extremely heavy precipitation, especially in urban areas, has increased signi-

ficantly in the past 60 years (Xiao et al., 2016). It has posed a serious threat to human life due to the increase in proportion of the urban population by 60% in 2020 ([http://www.gov.cn/zhengce/content/2017-01/25/content\\_5163309.htm](http://www.gov.cn/zhengce/content/2017-01/25/content_5163309.htm)). According to records from the past 10 years, extreme heavy rainfall in China has reported direct economic losses of approximately 1.7 trillion Yuan, accounting for approximately half of the losses from natural disasters in China (China Meteorological Administration, 2019). Therefore, extreme precipitation events and the associated influences need to be better un-

Supported by the National Natural Science Foundation of China (41521004, 41905013, and 41975088), Strategic Priority Research Program of Chinese Academy of Sciences (XDA2006010301), and China University Research Talents Recruitment Program [111 Project (B13045)].

\*Corresponding author: [hjp@lzu.edu.cn](mailto:hjp@lzu.edu.cn)

© The Chinese Meteorological Society and Springer-Verlag Berlin Heidelberg 2021

derstood as warming continues (Groisman et al., 2005; Min et al., 2011).

From 21 to 22 July 2012, an unprecedented extreme rainstorm event occurred in Beijing (hereinafter referred to as the “7.21” rainstorm). This rainfall event exceeded the historically recorded levels at several sites in Beijing, impacted 1.602 million people and caused 79 deaths and economic losses of 11.64 billion Yuan (<http://www.weather.com.cn/zt/kpzt/1696696.shtml>). Fang et al. (2012) simulated this event and found that the simulated time, intensity, and location of this typical rainstorm obviously deviated due to the uncertainties in the operational numerical model. For example, the start of the simulated precipitation was 6 h later than that of the actual rainfall, and the intensity was also significantly lower (Meng et al., 2019). Meng et al. (2019) noted that the main reasons for the failure of the extreme rainstorm simulation by the operational numerical model were the large biases in the simulations for the location and intensity of the low vortex and the associated low pressure trough. Moreover, this event was difficult to simulate due to the large uncertainties in the weather forecast models (Ye et al., 2006), and the current models are still unsatisfactory for simulating extreme heavy precipitation (e.g., Fang et al., 2012; Meng et al., 2019). These problems reveal that the study of extreme precipitation processes is not comprehensive and in-depth.

Generally, this extreme rainfall event was affected by the low-altitude mesoscale weather system, and the intensity and area of this event were mainly dependent on the movement of the mesoscale system (Zhang et al., 2017). Meanwhile, there are many other factors that are important for simulating extreme rainfall, including the physical and dynamical processes of the simulation range and selected geographic location (Miao et al., 2018). In addition, different surface conditions have an impact on the model simulation of precipitation, in which the high-precision surface data could improve the regional model simulation capability, e.g., the Weather Research and Forecasting (WRF) regional model (Pan et al., 2012). Urban areas exhibit obvious changes due to accelerating urbanization, influencing the urban precipitation distribution, and the area and intensity of precipitation by changing the transport and vertical movement of water vapor in the lower atmosphere (Zhang et al., 2007; Zheng et al., 2017). For the “7.21” rainstorm, a simulation with the urbanization effect could provide better precipitation distributions than site observations, and the changes in precipitation over some areas could reach more than 80–100 mm (Zheng, 2013). Therefore, the Moderate Resolution Imaging Spectroradiometer (MODIS) land-use type at

30” resolution was used in the current model to investigate the effect of rapid urban expansion in China.

In recent years, with the rapid development of numerical models, the parameterizations for physical processes and initial conditions have been continually improved, but systematic errors of models are still inevitable, which result in an accumulation of model errors during the integration process and large deviations in the simulation results. To solve this problem, the nudging assimilation method is applied in simulation processes (Stauffer and Seaman, 1990; Von Storch et al., 2000). This method can greatly reduce the systematic errors by adding a forcing term to the model and keeping the physical processes in dynamic balance. Meanwhile, the simulation results are continuously approximated to the analysis field or the observation field. Therefore, the accumulation of model errors during the integration process is limited, and the simulation deviation is reduced (Stauffer and Seaman, 1990; Von Storch et al., 2000). For example, Otte et al. (2012) studied whether nudging would inhibit the development of weather-scale information in a model when the deviation of the model results was limited to large-scale driving fields. The authors found that the nudging method did not restrain the simulations of extreme temperatures and precipitation, and it was a necessary condition for simulating extreme events. Therefore, using the nudging method in the model simulations is beneficial for understanding this extreme precipitation event.

Currently, there are two widely used nudging methods: grid nudging (GN) and spectral nudging (SN). However, the assimilation variables of the two methods are different, and their assimilation effects are affected by parameter settings such as assimilation intensity and height (e.g., Pohl and Crétat, 2014; Omrani et al., 2015; Tang et al., 2017). However, there is no unified conclusion regarding the superiority of the two nudging methods in simulating extreme precipitation. On the one hand, some studies have suggested that GN over-constrains regional climate models on a small scale as they approach large-scale driving fields (Castro et al., 2005), while SN can make the model simulate large- and small-scale fields in a balanced state by using different truncations (Von Storch et al., 2000). On the other hand, even with the default parameter settings, GN is more effective than SN in reducing the deviation of simulated meteorological factors in the WRF model on the ground and at different heights (Ma et al., 2016). When a proper nudging coefficient is selected, GN is generally better than SN, and the simulated precipitation intensity and frequency are close to the observations (Bowden et al., 2012; Otte et al.,

2012). In addition, current studies on GN and SN are mostly based on seasonal or above-scale weather or climate simulations, while there are few studies on extreme precipitation weather. Research on how the two methods improve the simulation of short-term extreme heavy precipitation still needs further exploration.

In this study, we will study the Beijing “7.21” rainstorm by using the WRF regional model. The urban surface (NU) data obtained from remote sensing retrievals were used to replace the default datasets in the WRF model. Then, the GN and SN schemes were conducted during the simulation, and their differences are discussed. To compare the differences in precipitation simulations in the different experiments, the threat score (TS), correlation coefficient (CC), and root mean square error (RMSE) of each group were used to evaluate the improvements caused by changing the NU and the two assimilation methods of GN and SN on extreme precipitation. By analyzing the accuracy of the spatial distribution patterns in the simulations at 500-hPa potential height and 850-hPa water vapor transport in each group, the reasons for the improvements to the simulation of extreme precipitation can be analyzed. Section 2 of this study introduces the model description; Section 3 presents the data and methods; Section 4 presents the model results and analysis; and Section 5 presents the conclusions and discussion.

## 2. Model description

### 2.1 WRF model

The WRF v3.5.1 (Skamarock et al., 2008) model is a mesoscale weather forecast model developed by the NCAR and NCEP. In this case, the model is configured with two one-way nested domains (Fig. 1). D01 covers most areas in China, north Indian Ocean, and western Pacific, and D02 covers Beijing and the surrounding areas where the extreme precipitation event occurred. The horizontal grid points are  $349 \times 299$  and  $400 \times 350$ , and the corresponding grid spacings are 20 and 4 km, respectively. The data for the initial field and the boundary field were from the NCEP final analysis (NCEP/FNL). The spatial resolution of the data was  $1^\circ \times 1^\circ$ , and the time interval was 6 h. The simulation time was from 0000 UTC 19 to 1800 UTC 23 July 2012.

The parameterization schemes including the RRTMG (rapid radiative transfer model for general circulation models) longwave and shortwave radiation solutions (Mlawer et al., 1997; Iacono et al., 2000), Morrison double-moment microphysical schemes (Morrison et al., 2009), Noah land surface process scheme (Chen and

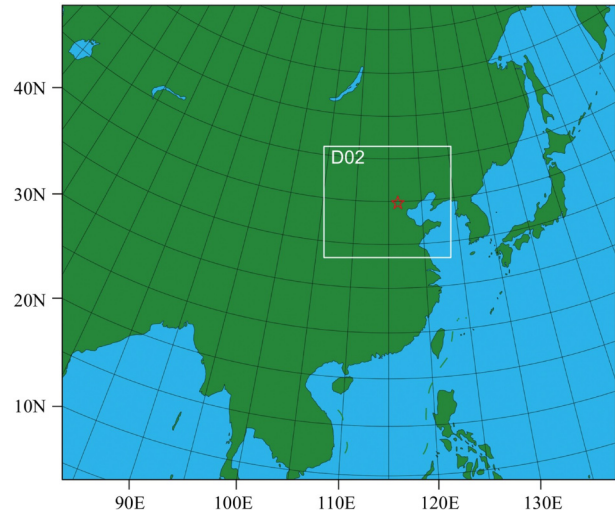


**Fig. 1.** Two one-way nested domain configuration. The red star is Beijing. The selected range of evaluation model results was  $39.45^\circ\text{--}41.1^\circ\text{N}$ ,  $115.4^\circ\text{--}117.4^\circ\text{E}$ .

Dudhia, 2001), YSU (Yonsei University) boundary layer scheme (Hong et al., 2006), Kain–Fritsch (new Eta) cumulus scheme (Kain, 2004), and MM5 (Mesoscale Model) Monin–Obukhov surface layer scheme (Monin and Obukhov, 1954) were selected in this study. Moreover, the nudging variables were the horizontal wind components ( $u$  and  $v$ ), potential temperature ( $T$ ), and water vapor mixing ratio ( $Q$ ) for GN, and were  $u$ ,  $v$ ,  $T$ , and geopotential height ( $H$ ) for SN. The nudging coefficients were set to  $0.0003 \text{ s}^{-1}$  for  $u$ ,  $v$ , and  $T$ , and  $0.00001 \text{ s}^{-1}$  for  $Q$  and  $H$  according to Mai et al. (2017, 2020). All nudging runs were applied above the planetary boundary layer. The cutoff wavenumbers for SN in the zonal and meridional directions were set to constant values of 3 (D01) and 1 (D02), which correspond to cutoff wavelengths of 2000 km (D01) and 1500 km (D02) considering scales of approximately 1500–2000 km and larger, respectively, and were reliable for the FNL analysis (Mai et al., 2020).

### 2.2 Nudging 4D assimilation

The core idea of the nudging method is to add a proportional spurious tendency term from the difference between the forecast and the real conditions in the prediction equation, which could push the model results closer to the observations and achieve dynamic coordination between the variables.

GN approximates the model results to the time-interpolated reanalysis data at each grid point. As stated by Stauffer and Seaman (1994), the principle equation can be expressed as follows:

$$\frac{da}{dt} = F(a,t) + G(a)w_a(a_i - a), \quad (1)$$

where  $a$  is the model variable, and  $a_i$  is the observed variable;  $F(a,t)$  refers to as the physical forcing term, and  $G(a)$  refers to as relaxation strength controlled by the time scale ( $G = 1/t'$ ,  $t'$  is the relaxation time scale, unit: s); and  $w_a$  indicates a general term for horizontal, vertical, and time weights.

$$\frac{da}{dt} = F(a,t) + G(a)w_a \sum_{|m| \leq N} \sum_{|n| \leq M} K_{mn}(a_{imn} - a_{mn})e^{ik_m x} e^{ik_n y}, \quad (2)$$

where  $m$  and  $n$  refer to as the truncated wavenumbers in the  $x$  and  $y$  directions, respectively;  $a_{imn}$  and  $a_{mn}$  represent the spectral coefficients of  $a$  and the observed variable of  $a_i$ , respectively;  $K_{mn}$  is a scale-dependent relaxation coefficient; and  $k_m$  and  $k_n$  are wave vector components in the  $x$  and  $y$  directions, respectively, and can be calculated by the following equations:

$$k_m = \frac{2\pi \cdot m}{D_x}, \quad k_n = \frac{2\pi \cdot n}{D_y}, \quad (3)$$

where  $D_x$  and  $D_y$  refer to as the size of the simulation area in the  $x$  and  $y$  directions, respectively.

### 2.3 Numerical experiments

Six groups of experiments (Table 1) were designed for the simulation study in this study:

(1) Control test (CTL): The default NU in the WRF model was used, and nudging was not used in the integration process;

(2) Test of replacing the NU: The default NU in the WRF model was replaced by the NU from remote sensing retrieval, and nudging was not used in the integration process;

(3) GN test in the outside domain (GN1): The default NU in the WRF model was replaced by the NU from remote sensing retrieval, and GN was used in the D01 model area during the integration process;

(4) GN test in the double nesting area (GN2): The default NU in the WRF model was replaced by the NU from remote sensing retrieval, and GN was used in the D01 and D02 model areas during the integration process;

(5) SN test in the outside domain (SN1): The default NU in the WRF model was replaced by the NU from remote sensing retrieval, and SN was used in the D01 model area during the integration process;

(6) SN test in the double nesting area (SN2): The default NU in the WRF model was replaced by the NU from remote sensing retrieval, and SN was used in the D01 and D02 model areas during the integration process.

## 3. Data and methods

### 3.1 Data

(1) The precipitation observations used in this study are the hourly gridded precipitation dataset (version 1.0) obtained by fusing the China automatic station and Climate Prediction Center (CPC) morphing (CMORPH) precipitation products provided by the China Meteorological Data Network. The datasets combine the observed hourly precipitation from 30,000 to 40,000 automatic weather stations nationwide after quality control and the global precipitation inversion product of the CMORPH satellite with a resolution of 8 km every 30 min developed by the U.S. Climate Prediction Center. The spatial resolution is  $0.1^\circ \times 0.1^\circ$ , and the temporal resolution is 1 h.

(2) The  $H$ , wind field, and water vapor transport field are derived from reanalysis data provided by the ECMWF. In this study,  $H$  at 500 hPa and the wind field and water vapor flux field at 850 hPa are analyzed. The spatial resolution is  $0.5^\circ \times 0.5^\circ$ , and the temporal resolution is 6 h.

(3) Remote sensing retrievals of urban underlying surface data include Cropland Extent 1 km Crop Dominance, Global Food-Support Analysis Data (GFSAD1000; [Thenkabail et al., 2012](#)), and MODIS Land Cover Type Yearly Global 500 m (MODIS MCD12Q1) products ([Friedl et al., 2002](#)). Moreover, there are six different classification schemes in the MCD12Q1 product ([Di Gregorio and Jansen, 2005](#)), in which the two schemes of the Food and Agriculture Organization (FAO) Land Cover Classification System (LCCS) land cover and FAO LCCS surface hydrology are used.

In this study, the surface type data (real surface type data) retrieved by remote sensing are used to replace the default data in the WRF model. [Figure 2a](#) shows the original surface type data in the WRF model. The red part means that the urban area is very small, which seriously deviates from the actual range of the urban area. [Figure 2b](#) shows the updated NU replaced in this simulation test, which best reflects the urban distribution. In this study, the Beijing area ( $39.45^\circ$ – $41.1^\circ$ N,  $115.4^\circ$ – $117.4^\circ$ E) was

**Table 1.** Model test design

Name	D01		D02	
	Land-use category	Nudging	Land-use category	Nudging
CTL	Default	No	Default	No
NU	New	No	New	No
GN1	New	Yes	New	No
GN2	New	Yes	New	Yes
SN1	New	Yes	New	No
SN2	New	Yes	New	Yes

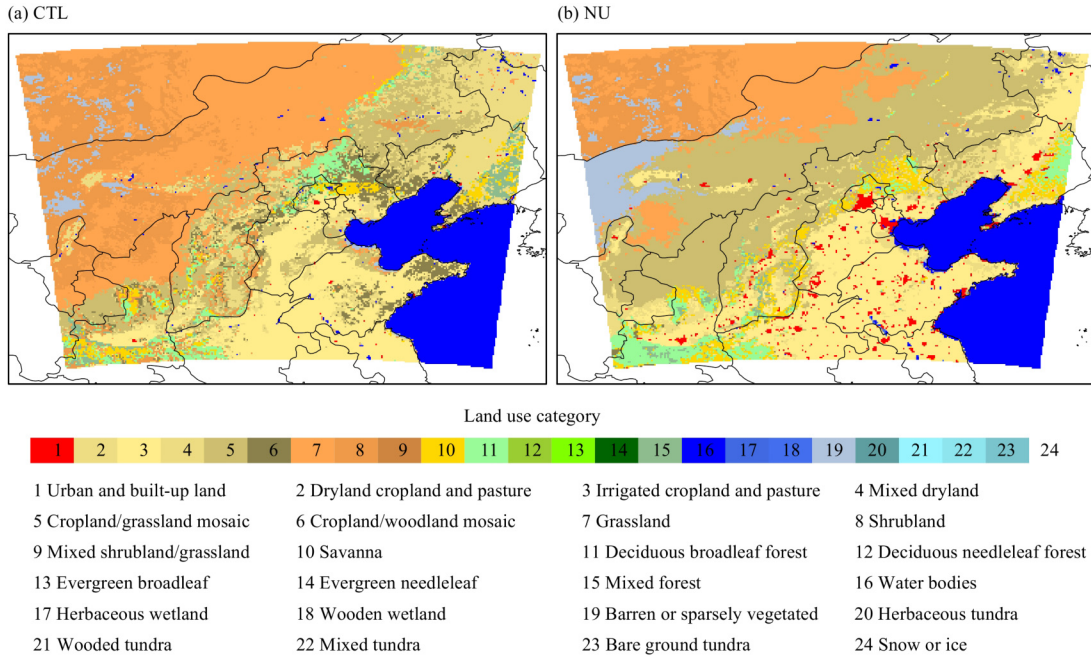


**Fig. 2.** (a) Default surface types in the control test (CTL) and (b) surface types retrieved from remote sensing in the real urban surface (NU) test (red blocks represent cities).

selected to evaluate the simulation results of extreme heavy rainfall in different model tests.

### 3.2 Evaluation methods

To evaluate the simulation effect of the model on precipitation, the statistical methods used in this study are as follows:

$$\text{Mean error (ME)} : \text{ME} = \bar{p} - \bar{o}, \quad (4)$$

$$\text{RMSE} : \text{RMSE} = \sqrt{\frac{1}{N} \sum_{i=1}^N (p_i - o_i)^2}, \quad (5)$$

$$\text{CC} : \text{CC} = \frac{\frac{1}{N-1} \left[ \sum_{i=1}^N (p_i - \bar{p})(o_i - \bar{o}) \right]}{\left[ \frac{1}{N-1} \left[ \sum_{i=1}^N (p_i - \bar{p})^2 \right] \right]^{1/2} \left[ \frac{1}{N-1} \left[ \sum_{i=1}^N (o_i - \bar{o})^2 \right] \right]^{1/2}}, \quad (6)$$

where  $N$  refers to as the sample number,  $p_i$  represents the result of the model,  $o_i$  represents the observed value, and  $\bar{p}$  and  $\bar{o}$  represent the average value of the simulation results and the observed values, respectively.

$$\text{TS score} : \text{TS} = \frac{a}{a+b+c}. \quad (7)$$

The TS score reflects the accuracy of forecasted precipitation at a certain level. The value of the TS score is between 0 and 1. The closer the TS value is to 1, the better the forecast effect will be; in contrast, the closer it is

to 0, the worse the forecast effect will be. The events represented by  $a$ ,  $b$ , and  $c$  are shown in Table 2.

## 4. Model result analysis

### 4.1 Observation and analysis of July 21 rainstorm in Beijing

Observation data of the 6-h average precipitation on July 21 (Fig. 3) showed that the rainfall in Beijing was mainly concentrated from 0600 to 1200 UTC, during which the precipitation exceeded 100 mm. The precipitation intensity in southwestern Beijing was highest with a long duration. From 0400 to 0900 UTC, precipitation decreased in some parts of Beijing, but there was still more than 100-mm precipitation in Beijing and the surrounding areas. After that, the eastward shift of the rainfall cloud clusters weakened, and the heavy rain process was basically over. Until 1600 UTC, according to the observation data from 20 national observation stations in Beijing, heavy rainstorms occurred in most areas of Beijing, and precipitation in parts of southwestern Beijing had reached the level of an extreme rainstorm. During this event, the average precipitation in Beijing was 170 mm, and the average precipitation in the urban

**Table 2.** Classification of precipitation test

Fact/forecast	Exist	None
Exist	$a$	$c$
None	$b$	—

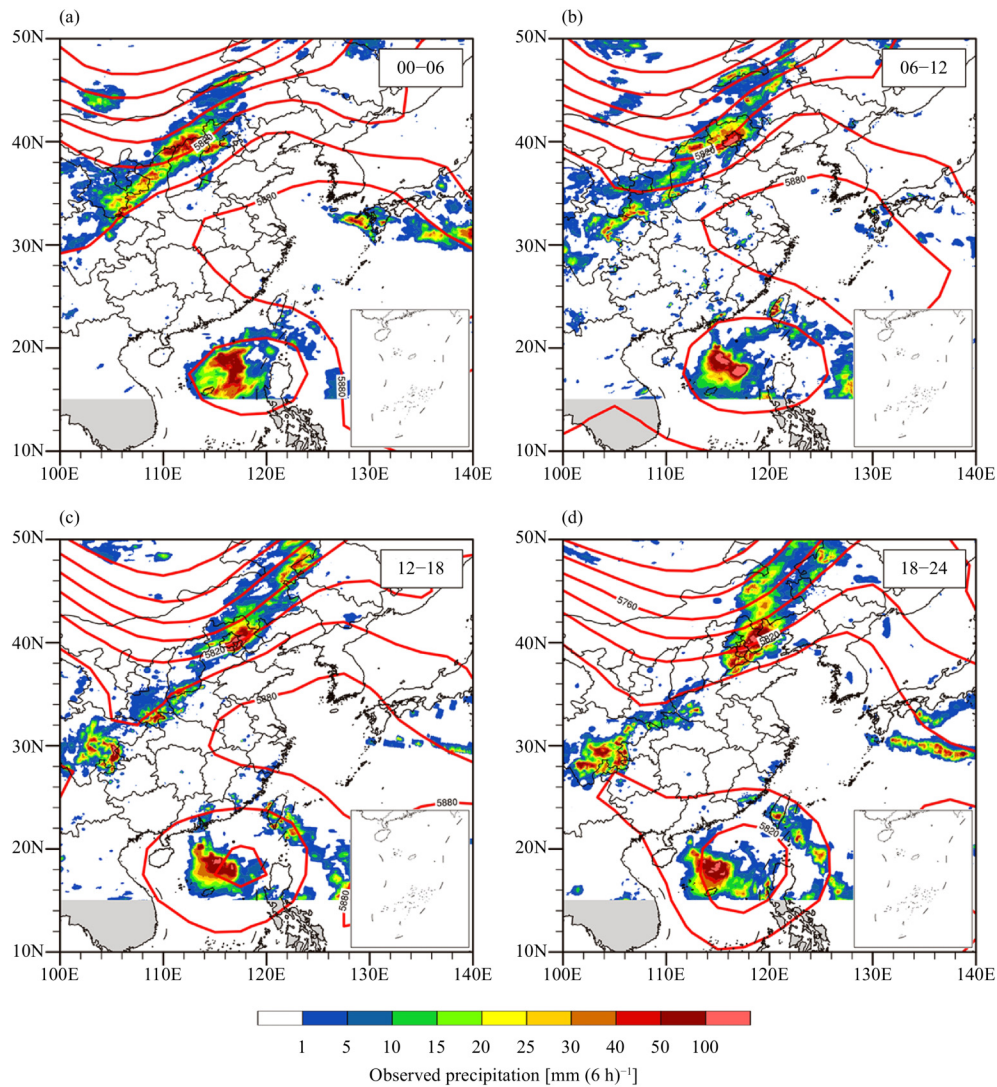


**Fig. 3.** Six-hour cumulative precipitation and 500-hPa geopotential height field at (a) 0000–0600, (b) 0600–1200, (c) 1200–1800, and (d) 1800–2400 UTC 21 July. The coloring represents accumulated precipitation [ $\text{mm} (6 \text{ h})^{-1}$ ], and the red solid line represents the 500-hPa geopotential height field (gpm).

area was 215 mm. In Hebei town of Fangshan District (hydrological station), the average precipitation was 460 mm. The maximum rainfall in the urban area of Beijing occurred at Shijingshan, reaching 328 mm.

According to the 6-h average circulation data from 0000 to 0600 UTC July 21 (Fig. 3), the main parts of the western Pacific subtropical high were located in the middle and lower reaches of the Yangtze River and the ocean surface to its east in China. After that, the 5880-gpm control area was gradually narrowed, and the subtropical high gradually weakened and retreated to the east of 130°E. The high-altitude trough from Lake Baikal to northern China gradually deepened and slowly moved eastward. From 1200 to 1800 UTC, Beijing was in front of the trough bottom, which was beneficial for precipitation, and between 1800 and 2400 UTC, as the high-alti-

tude trough continued to move eastward, the transit of the upper-air trough and precipitation in Beijing gradually weakened. In Fig. 4, the water vapor flux at 850 hPa shows that there was a strong water vapor northward conveyor route from western Huanghuai River basin to southern North China during 0000–0600 UTC, which formed a cyclonic circulation with the dry cold airflow on the northwest side in the east of the western region. From 0600 to 1600 UTC, the cyclonic circulation moved eastward to western North China, and the intensity was further strengthened. Water vapor in front of the cyclone began to affect Beijing. From 1200 to 1800 UTC, Beijing was in front of the cyclonic circulation, and the maximum water vapor conveyor route covered this area; thus, the precipitation reached its highest value in this phase. From 1800 to 2400 UTC, the cyclonic circulation and the

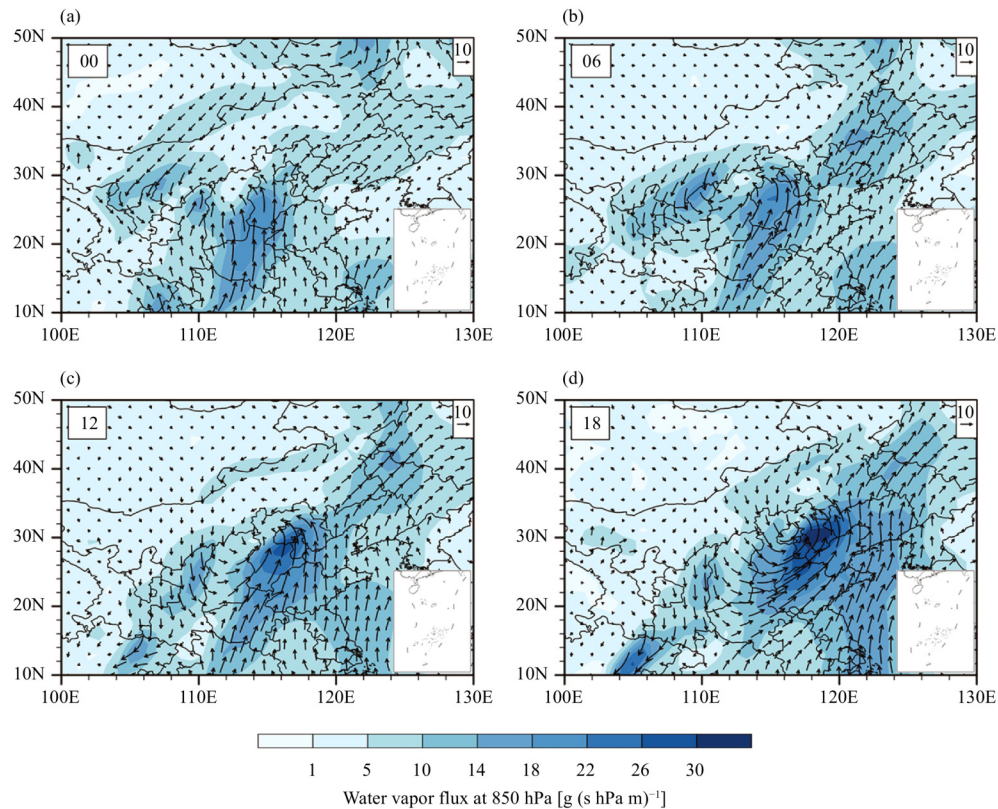


**Fig. 4.** Six-hour average 850-hPa water vapor transport at (a) 0000, (b) 0600, (c) 1200, and (d) 1800 UTC 21 July. The coloring represents the water vapor flux, and the arrow represents the water vapor flux vector [unit:  $\text{g (s hPa m)}^{-1}$ ].

strong water vapor conveyor moved further to the east and north with a weak impact on Beijing.

#### 4.2 Precipitation simulation

Figure 5 shows the hourly precipitation intensity in the analysis area defined in Fig. 1 and the simulations from the six groups of experiments. The CTL of the heavy rain exhibited a large deviation from the actual observations in the simulation of the precipitation peak and hourly precipitation intensity (Fig. 5). The maximum simulated rainfall intensity was  $19 \text{ mm h}^{-1}$ , far exceeding the actual maximum observed value of  $15 \text{ mm h}^{-1}$ , but the occurrence time was the early morning of the next day, which was also delayed from the observed peak moment between 1300 and 1400 UTC. The simulated value of the maximum precipitation per hour in the NU test was close to the actual observed value of  $15 \text{ mm h}^{-1}$ , but the simulation of the precipitation intensity in this group of tests still showed a monotonous increasing trend, and the simulation of the precipitation peak had the same deficiencies as the CTL. SN1 and SN2 failed to simulate the hourly precipitation during this heavy rain event, and the maximum hourly precipitation was only  $4 \text{ mm h}^{-1}$ . GN1 and GN2 could better simulate the actual conditions of precipitation than the other experiments. From the hourly

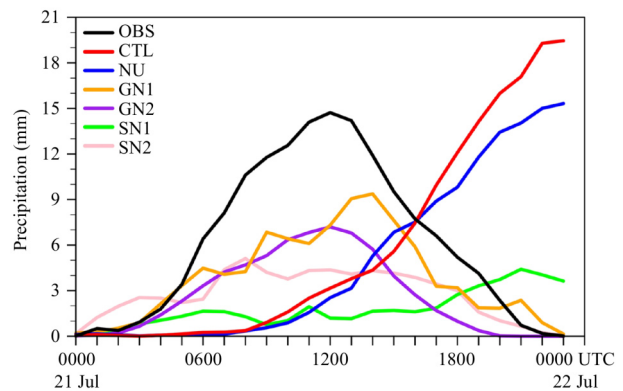


**Fig. 5.** Hourly precipitation intensity from six models' rainfall simulation results and from observations (OBS) during 0000 UTC 21–0000 UTC 22 July.

precipitation intensity changes, GN2 failed to show the corresponding precipitation peak in the simulation results of the whole precipitation process, and the whole precipitation process was relatively smooth. The simulation of the hourly precipitation process by GN1 was not so accurate as that by GN2, but in this test, the simulation of the maximum hourly precipitation of  $9 \text{ mm h}^{-1}$  was closest to the actual observation, and the simulated peak moment was only 1.5 h behind.

The differences among the hourly precipitation values of the six groups of nudging experimental simulation results and the observation data are provided in Fig. 6a. The results showed that the precipitation peaks of the six groups of simulation experiments were relatively small, and GN1 and GN2 exhibited the smallest deviation from the precipitation simulation (the maximum deviation was less than  $8 \text{ mm h}^{-1}$ ), while the maximum errors of the four groups of comparative tests of SN1, SN2, CTL, and NU exceeded  $10 \text{ mm h}^{-1}$ . The TS score (Fig. 6b), CC (Fig. 6c), and RMSEs (Fig. 6d) between the observed and simulated precipitation also showed that the simulations of GN1 and GN2 were closest to the actual precipitation observations.

#### 4.3 Analysis of precipitation conditions

As represented by the 500-hPa  $H$  field, the simulated subtropical high by the CTL and NU (Fig. 7) was weak compared with the actual reanalysis data (Fig. 3). Additionally, the range of 5880 gpm was relatively small, and the location exhibited a southward and eastward shift. Correspondingly, the northern high-altitude trough was developing in depth and moving slowly, resulting in the delayed arrival of the rain zone in Beijing. At the peak of the actual precipitation intensity between 1200 and 1800

UTC, the northern high-altitude trough was located westward of the observations, and the main rain zone had not yet reached Beijing. At this time, the high-altitude trough was still gradually deepening. From 1800 to 2400 UTC, Beijing was in front of the deepened high-altitude trough; thus, lagging and strong precipitation was presented by the simulations during this period. SN2 and SN1 (Fig. 8) were close to the actual subtropical high intensity. The 5880-gpm range was slightly wider than the observations, but the overall location exhibited a westward and northward shift, which caused the location of the north upper trough to move northward, the overall location to be shallow and the intensity to be weak. Therefore, GN2 and GN1 (Fig. 9) were closer to the simulation of the subtropical high than SN2 and SN1, but the simulations of the northern high-altitude trough by SN2 and SN1 were closer to the actual situation. Especially between 1200 and 1800 UTC, the deviation of the location and intensity of the high-altitude trough was less than the actual condition. Therefore, this result may be one of the reasons why the peak precipitation simulations of GN1 and GN2 were close to the observations.

Comparing the water vapor transport flux at 850 hPa, the simulations of the location of cyclonic circulation and the strong water vapor conveyor by the CTL and NU

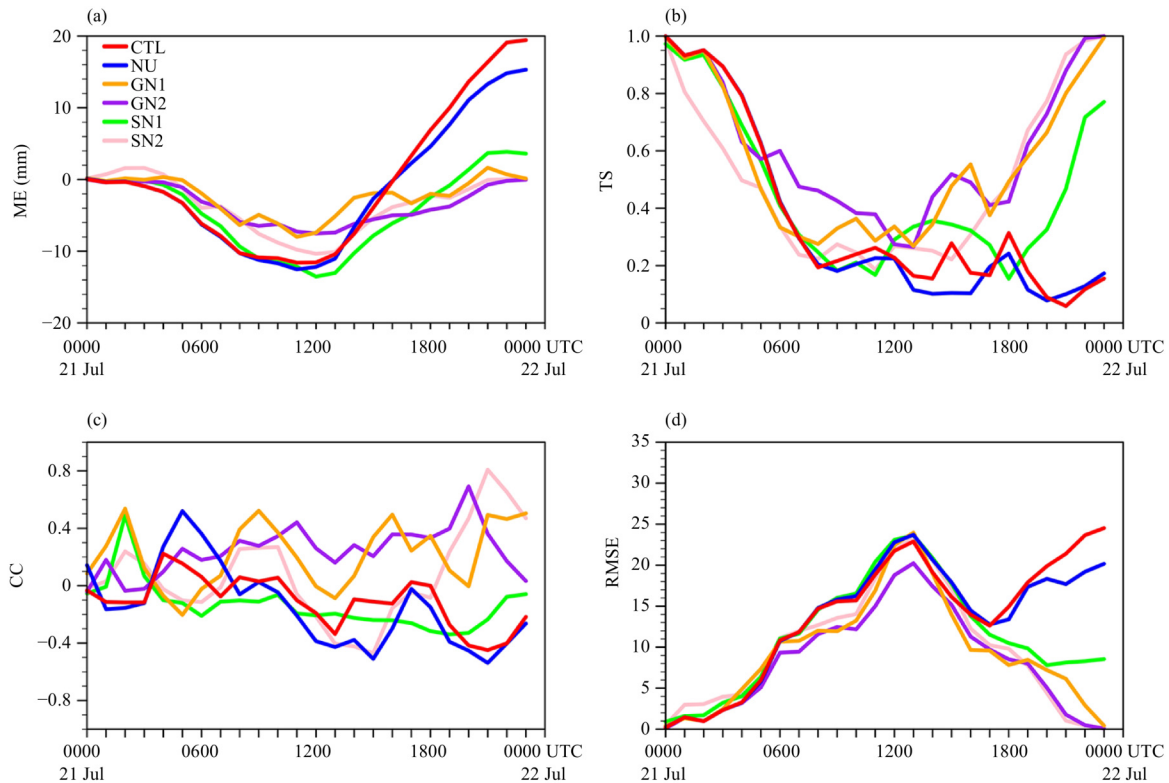


**Fig. 6.** Hourly precipitation differences among the six groups of experimental simulation results and observation data for (a) mean error (ME), (b) TS score, (c) CC, and (d) RMSE from 0000 UTC 21 to 0000 UTC 22 July.

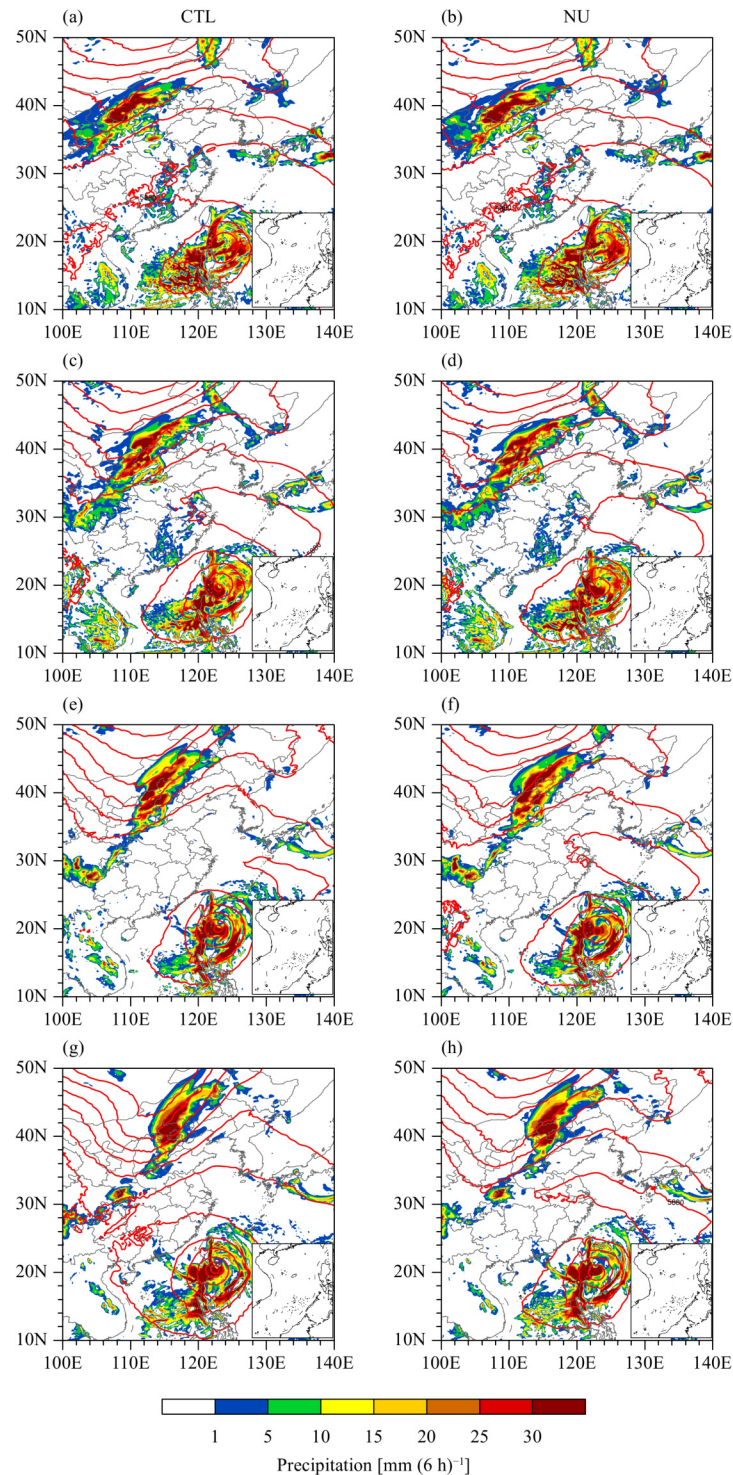


**Fig. 7.** Six-hour precipitation simulations [ $\text{mm (6 h)}^{-1}$ ] of (a, c, e, g) the CTL and (b, d, f, h) NU during (a, b) 0000–0600, (c, d) 0600–1200, (e, f) 1200–1800, and (g, h) 1800–2400 UTC 21 July. The red solid line indicates the geopotential height field (gpm).

were slowly moving south (Fig. 10). During the peak period of actual precipitation intensity between 1200 and 1800 UTC, the location of the cyclonic circulation and the strong water vapor conveyor in the front exhibited a westward and southward shift, which had a weak impact on Beijing. This shift gradually affected Beijing from

1800 to 2400 UTC. Therefore, the simulation of the precipitation occurrence time was late. Between 1200 and 1800 UTC, the position of the strong water vapor conveyor simulated by SN2 was eastward of the observations, and the main part was east of Beijing, which led to a weak impact on the precipitation in Beijing. The strong

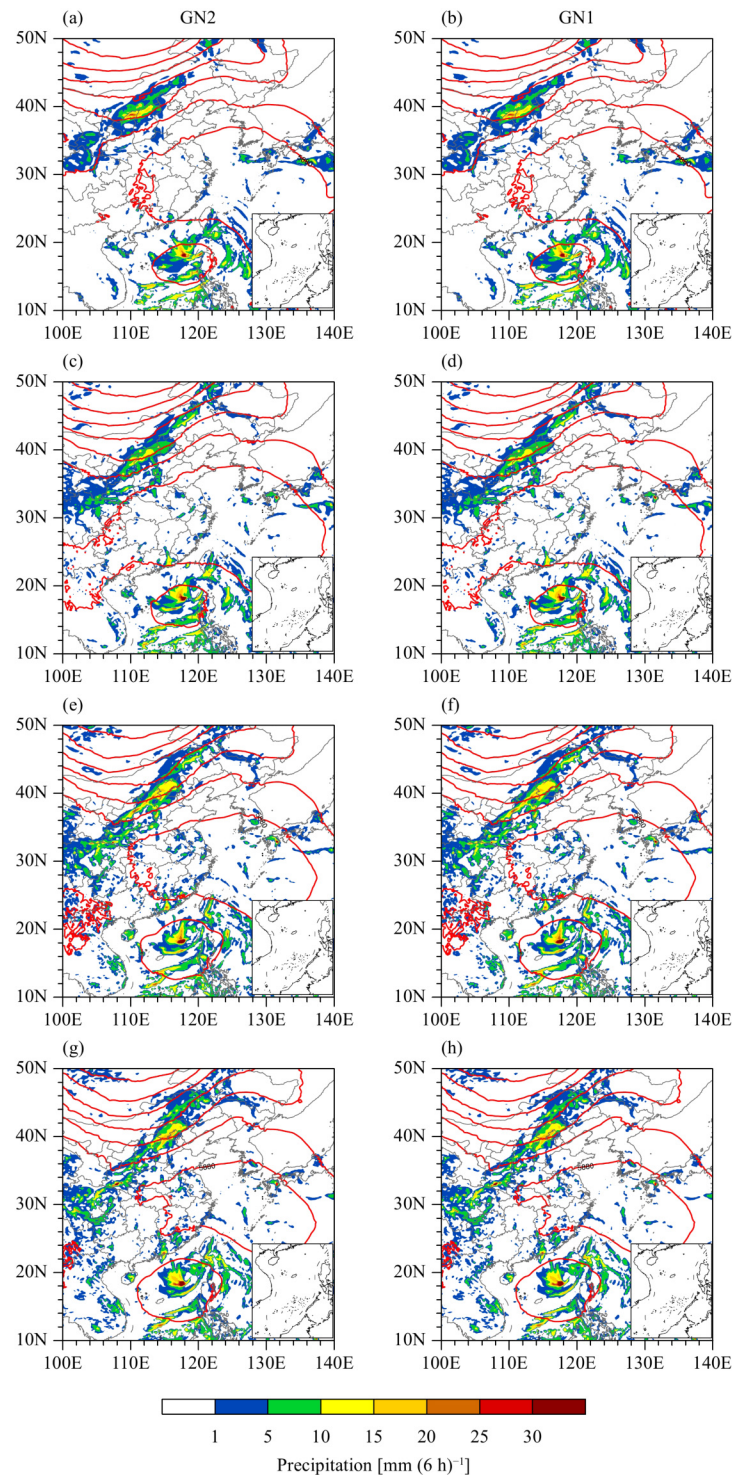


**Fig. 8.** As in Fig. 7, but for SN2 and SN1.

water vapor conveyor from SN1 was transported to the north, with a maximum value centered over northern Beijing. The enhancements of SN2 and SN1 (Fig. 11) in terms of cyclonic circulation and their impact on Beijing were mainly at and after 1800–2400 UTC; thus, the simulation of precipitation lagged and was prolonged. The GN2 and GN1 simulations (Fig. 12) of the strong water

vapor conveyor were better than those of SN2 and SN1. Between 0600 and 1200 UTC, the simulations of cyclonic circulation and the water vapor conveyor were close to the actual situation. Therefore, the deviation between the simulation and the actual situation of precipitation at this time was relatively small. However, from 1200 to 1800 UTC, the simulation of the cyclonic circulation intensity

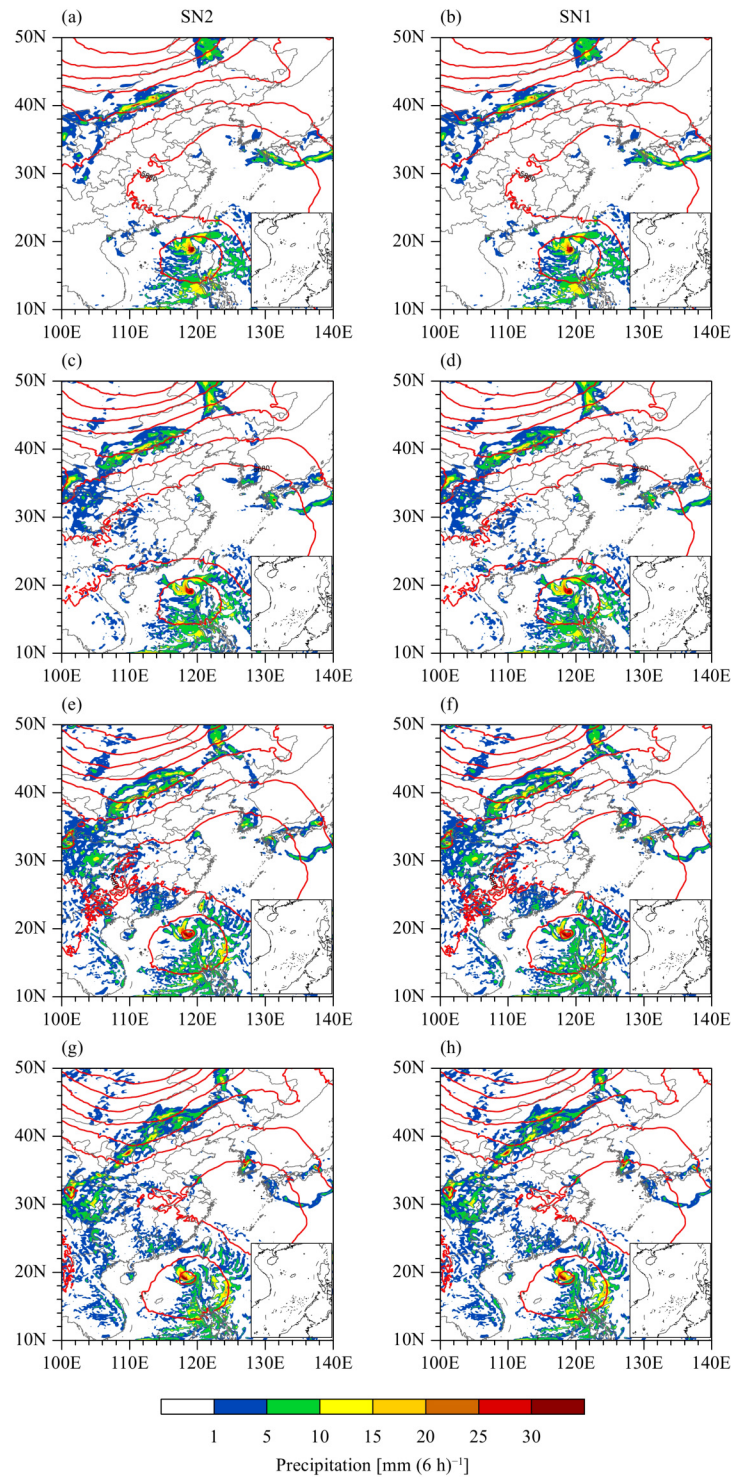
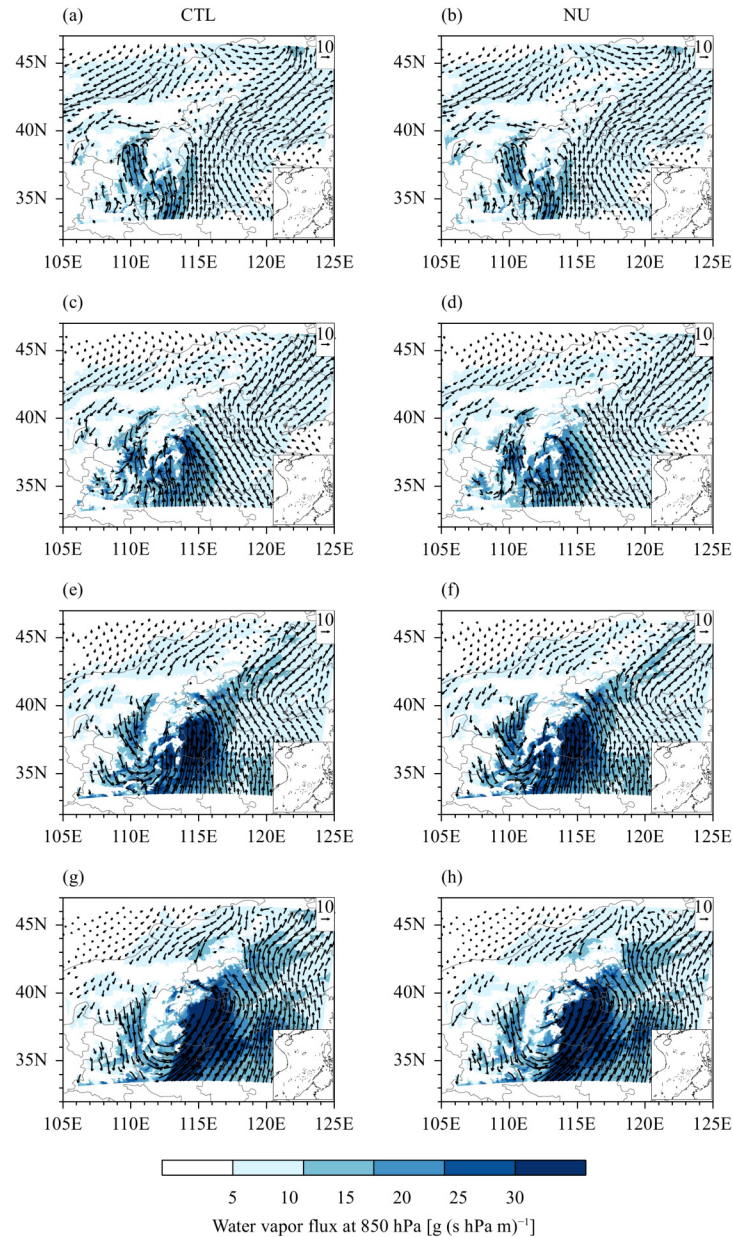


Fig. 9. As in Fig. 7, but for GN2 and GN1.

was weak. The position simulated in the GN1 simulation and the intensity of the cyclonic circulation and the strong water vapor conveyor belt exhibited less deviation from the actual situation; thus, it could simulate the occurrence of precipitation peaks better than the other experiments. The location of the strong water vapor conveyor in the GN2 simulation was eastward of the obser-

variations. Therefore, the precipitation simulated by GN2 was weaker than that simulated by GN1 over the whole area.

In summary, GN1 and GN2 exhibited the best simulations of the high-altitude trough and subtropical high that affected precipitation in Beijing. The simulated water vapor transport fields and low cyclones were also more ac-



**Fig. 10.** As in Fig. 7, but for average water vapor flux simulation of the CTL and NU. The coloring indicates the water vapor flux, and the arrow is the water vapor flux vector [ $\text{g (s hPa m)}^{-1}$ ] on July 21.

curate than those in the other experiments. The SN1 and SN2 simulated subtropical high intensities were close to the actual situation, but the northern high-altitude trough was relatively poor, and the simulated location and intensity of the water vapor conveyor were also relatively poor. The CTL and NU tests had poor capacity to simulate the subtropical high, and the simulated locations of cyclonic circulation and the strong water vapor conveyor route were southward compared with the observations and moved slowly; therefore, the simulated previous precipitation was weak, and the peak moment lagged.

## 5. Conclusions and discussion

In this study, six groups of experiments based on the WRF model were carried out to simulate a heavy rain event in Beijing by using the data from the urban underlying surface acquired by remote sensing retrieval instead of the default urban underlying surface of the WRF model and nudging method. The results are summarized as follows:

(1) In terms of the TS score (Fig. 6b), there was no significant difference except in SN2 in the early stage of precipitation. The GN2 and GN1 scores were the highest

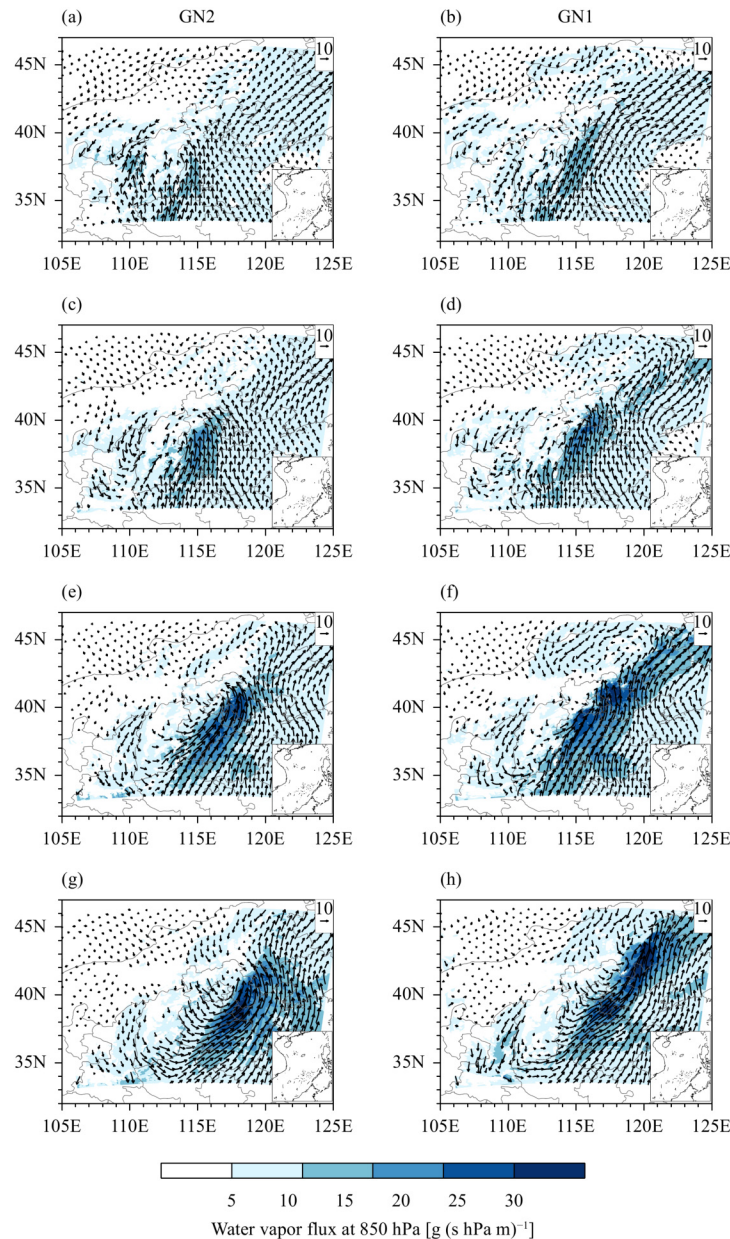
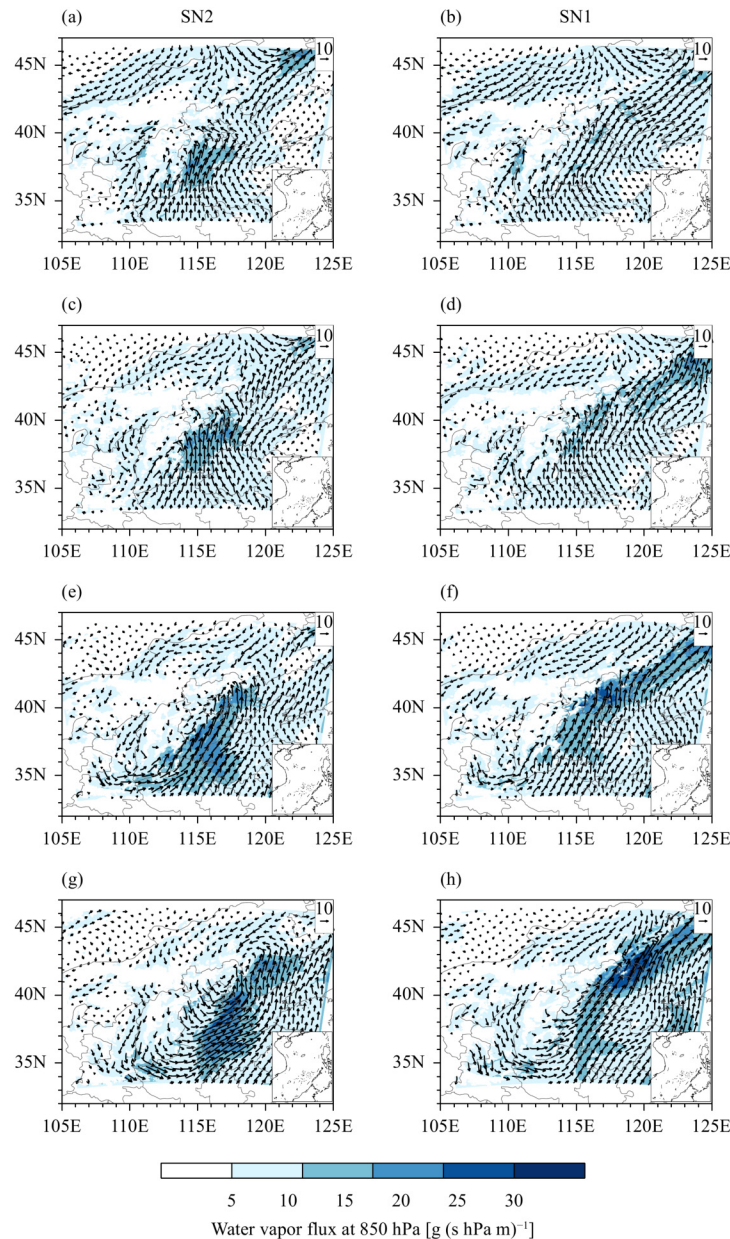


Fig. 11. As in Fig. 10, but for SN2 and SN1.

in the main precipitation periods; SN1 was relatively high for a few times, and the rest were relatively low. In the late period of precipitation, the SN2, GN2, and GN1 scored the highest, and the rest were low. The CC skill scores indicated that the simulation of precipitation peaks (time distribution) in GN1 (GN2) was better than that in GN2 (GN1). The SN1, SN2, CTL, and NU tests were basically negatively correlated with the observation results. According to the comparison of RMSEs, GN2 had relatively small values at all times, and GN1 had relatively small values most of the time except at approximately 1300 UTC. Following SN2, the rest of the experiments had relatively large values. Therefore, in this case, the

simulation of this precipitation event by GN was closest to the real situation.

(2) The simulation of the heavy rain process by directly using the WRF model deviated greatly from the observations in the precipitation area, where the precipitation intensity decreased and the peak moment of precipitation seriously lagged. The CTL test mainly had the following three main problems: (i) the range and magnitude of water vapor transport were significantly larger than those of the reanalysis data; (ii) the circulation simulation affected the area and time of precipitation; and (iii) the weak 5880-gpm  $H$  field and the slow-moving and deep-developing northern high-altitude trough combined



**Fig. 12.** As in Fig. 10, but for GN2 and GN1.

with the strong transport of water vapor made the simulated precipitation stronger and later than the observed precipitation. Although the replacement of the default urban underlying surface in the WRF model made the peak of precipitation closer to the actual observation, the NU did not effectively improve the water vapor flux and circulation simulation in the CTL test. The reason was that extreme rainfall events were mainly dominated by high- and low-level weather systems and were less affected by local urban characteristics.

(3) GN was better at simulating precipitation than SN. In the case where the circulations were similar in GN1 and GN2, GN1 could better simulate the peak value of

precipitation. Because GN2 could adequately simulate  $H$  at 500 hPa, the 850-hPa water vapor transport, and the low-level cyclone system, the simulated spatial distribution of precipitation was more accurate, and the results were better than those of GN1.

(4) Although the simulated circulation patterns by the two SN tests and the two GN tests were similar, the precipitation intensity was seriously weaker than the actual situation due to the weak 850-hPa water vapor transport and the weak low air cyclone system. The two groups of SN tests exhibited large deviations from the observed values in the simulations of precipitation and meteorological element fields and could not simulate this extreme

precipitation process well. It could be concluded that the SN scheme was not applicable to this extreme precipitation event.

(5) The standard experiment (CTL) showed that the WRF model was not accurate enough to simulate both large- and small-scale weather systems. The GN and SN simulations of precipitation both had a certain deviation from the observation. However, SN restricted the large-scale weather system, while GN added constraints on the small-scale weather system based on the large-scale weather system, contributing to the improved simulations. This study also showed that the Beijing “7.21” heavy rainfall was caused by the large-scale circulation field combined with the abnormal low-altitude weather system. In addition, the deviation between the GN simulation and the observation may have resulted from the inaccuracy of the small-scale driving field system. The applications of a driving field with higher resolution and more complete small-scale information will be helpful to improve the simulations.

Overall, although the nudging assimilation method improved the simulations of this extreme precipitation event, the effects were limited. This finding may be caused by the failure to accurately simulate the abnormal circulation pattern and meteorological elements that caused extreme precipitation events, as well as the states of high and low circulation. However, this study provides a new scheme for the simulation of extreme precipitation and concludes that GN could be more applicable than SN for similar cases of extreme precipitation.

## REFERENCES

- Bowden, J., T. L. Ote, C. G. Nolte, et al., 2012: Examining interior grid nudging techniques using two-way nesting in the WRF model for regional climate modeling. *J. Climate*, **25**, 2805–2823, doi: [10.1175/JCLI-D-11-00167.1](https://doi.org/10.1175/JCLI-D-11-00167.1).
- Castro, C. L., R. A. Pielke Sr, and G. Leoncini, 2005: Dynamical downscaling: Assessment of value retained and added using the regional atmospheric modeling system (RAMS). *J. Geophys. Res. Atmos.*, **110**, D05108, doi: [10.1029/2004JD004721](https://doi.org/10.1029/2004JD004721).
- Chen, F., and J. Dudhia, 2001: Coupling an advanced land surface-hydrology model with the Penn State–NCAR MM5 modeling system. Part II: Preliminary model validation. *Mon. Wea. Rev.*, **129**, 587–604, doi: [10.1175/1520-0493\(2001\)129<0587:caalsh>2.0.co;2](https://doi.org/10.1175/1520-0493(2001)129<0587:caalsh>2.0.co;2).
- China Meteorological Administration, 2019: *Yearbook of Meteorological Disasters in China (2018)*. China Meteorological Press, Beijing, 229 pp. Available online at <https://navi.cnki.net/KNav/YearbookDetail?pcode=CYFD&pykm=YQXZH&bh>. Accessed on 23 November 2020. (in Chinese)
- Ding, Y. H., 1994: Some aspects of rainstorm and mesoscale meteorology. *Acta Meteor. Sinica*, **52**, 274–284. (in Chinese)
- Di Gregorio, A., and L. J. M. Jansen, 2005: Land Cover Classification System: Classification Concepts and User Manual. Food and Agriculture Organization of the United Nations, Rome, Italy, 163 pp.
- Fang, C., D. Y. Mao, X. W. Zhang, et al., 2012: Analysis on the mesoscale convective conditions and characteristics of an extreme torrential rain in Beijing on 21 July 2012. *Meteor. Mon.*, **38**, 1278–1287, doi: [10.7519/j.issn.1000-0526.2012.10.014](https://doi.org/10.7519/j.issn.1000-0526.2012.10.014). (in Chinese)
- Friedl, M. A., D. K. McIver, J. C. F. Hodges, et al., 2002: Global land cover mapping from MODIS: Algorithms and early results. *Remote Sens. Environ.*, **83**, 287–302, doi: [10.1016/S0034-4257\(02\)00078-0](https://doi.org/10.1016/S0034-4257(02)00078-0).
- Groisman, P. Y., R. W. Knight, D. R. Easterling, et al., 2005: Trends in intense precipitation in the climate record. *J. Climate*, **18**, 1326–1350, doi: [10.1175/JCLI3339.1](https://doi.org/10.1175/JCLI3339.1).
- Hong, S.-Y., Y. Noh, and J. Dudhia, 2006: A new vertical diffusion package with an explicit treatment of entrainment processes. *Mon. Wea. Rev.*, **134**, 2318–2341, doi: [10.1175/MWR3199.1](https://doi.org/10.1175/MWR3199.1).
- Iacono, M. J., E. J. Mlawer, S. A. Clough, et al., 2000: Impact of an improved longwave radiation model, RRTM, on the energy budget and thermodynamic properties of the NCAR community climate model, CCM3. *J. Geophys. Res. Atmos.*, **105**, 14873–14890, doi: [10.1029/2000JD900091](https://doi.org/10.1029/2000JD900091).
- Kain, J. S., 2004: The Kain–Fritsch convective parameterization: An update. *J. Appl. Meteor. Climatol.*, **43**, 170–181, doi: [10.1175/1520-0450\(2004\)043<0170:tkcpau>2.0.co;2](https://doi.org/10.1175/1520-0450(2004)043<0170:tkcpau>2.0.co;2).
- Kharin, V. V., F. W. Zwiers, X. Zhang, et al., 2007: Changes in temperature and precipitation extremes in the IPCC ensemble of global coupled model simulations. *J. Climate*, **20**, 1419–1444, doi: [doi:10.1175/JCLI4066.1](https://doi.org/10.1175/JCLI4066.1).
- Ma, Y. Y., Y. Yang, X. P. Mai, et al., 2016: Comparison of analysis and spectral nudging techniques for dynamical downscaling with the WRF model over China. *Adv. Meteor.*, 4761513, doi: [10.1155/2016/4761513](https://doi.org/10.1155/2016/4761513).
- Mai, X. P., Y. Y. Ma, Y. Yang, et al., 2017: Impact of grid nudging parameters on dynamical downscaling during summer over mainland China. *Atmosphere*, **8**, 184, doi: [10.3390/atmos8100184](https://doi.org/10.3390/atmos8100184).
- Mai, X. P., X. B. Qiu, Y. Yang, et al., 2020: Impacts of spectral nudging parameters on dynamical downscaling in summer over mainland China. *Front. Earth Sci.*, **8**, 574754, doi: [10.3389/feart.2020.574754](https://doi.org/10.3389/feart.2020.574754).
- Meng, Z. Y., X. J. Tang, J. Yue, et al., 2019: Impact of EnKF surface and rawinsonde data assimilation on the simulation of the extremely heavy rainfall in Beijing on July 21, 2012. *Acta Sci. Nat. Univ. Pekinensis*, **55**, 237–245. (in Chinese)
- Miao, W. H., H. C. Zuo, and L. Shu, 2018: Impact of nudging data assimilation method on the simulation of precipitation process in arid regions of Northwest China by WRF model. *Gansu Sci. Technol.*, **34**, 4–9, doi: [10.3969/j.issn.1000-0952.2018.12.003](https://doi.org/10.3969/j.issn.1000-0952.2018.12.003). (in Chinese)
- Min, S.-K., X. Zhang, F. W. Zwiers, et al., 2011: Human contribution to more-intense precipitation extremes. *Nature*, **470**, 378–381, doi: [10.1038/nature09763](https://doi.org/10.1038/nature09763).
- Mlawer, E. J., S. J. Taubman, P. D. Brown, et al., 1997: Radiative transfer for inhomogeneous atmospheres: RRTM, a validated correlated-k model for the longwave. *J. Geophys. Res.*

- Atmos.*, **102**, 16663–16682, doi: [10.1029/97JD00237](https://doi.org/10.1029/97JD00237).
- Monin, A. S., and A. M. Obukhov, 1954: Basic laws of turbulent mixing in the surface layer of the atmosphere. *Tr. Akad. Nauk SSSR Geofiz. Inst.*, **24**, 163–187.
- Morrison, H., G. Thompson, and V. Tatarskii, 2009: Impact of cloud microphysics on the development of trailing stratiform precipitation in a simulated squall line: Comparison of one- and two-moment schemes. *Mon. Wea. Rev.*, **137**, 991–1007, doi: [10.1175/2008MWR2556.1](https://doi.org/10.1175/2008MWR2556.1).
- Omrani, H., P. Drobinski, and T. Dubos, 2015: Using nudging to improve global–regional dynamic consistency in limited-area climate modeling: What should we nudge? *Climate Dyn.*, **44**, 1627–1644, doi: [10.1007/s00382-014-2453-5](https://doi.org/10.1007/s00382-014-2453-5).
- Otte, T. L., C. G. Nolte, M. J. Otte, et al., 2012: Does nudging squelch the extremes in regional climate modeling? *J. Climate*, **25**, 7046–7066, doi: [10.1175/JCLI-D-12-00048.1](https://doi.org/10.1175/JCLI-D-12-00048.1).
- Pan, X. D., X. Li, Y. H. Ran, et al., 2012: Impact of underlying surface information on WRF modeling in Heihe River basin. *Plateau Meteor.*, **31**, 657–667, doi: [10.1007/s11783-011-0280-z](https://doi.org/10.1007/s11783-011-0280-z). (in Chinese)
- Paul, A. O., and S. Tapio, 2009: The physical basis for increases in precipitation extremes in simulations of 21st-century climate change. *Proc. Natl. Acad. Sci. USA*, **106**, 14773–14777, doi: [10.1073/pnas.0907610106](https://doi.org/10.1073/pnas.0907610106).
- Pohl, B., and J. Cr  tat, 2014: On the use of nudging techniques for regional climate modeling: Application for tropical convection. *Climate Dyn.*, **43**, 1693–1714, doi: [10.1007/s00382-013-1994-3](https://doi.org/10.1007/s00382-013-1994-3).
- Skamarock, W. C., J. B. Klemp, J. Dudhia, et al., 2008: A Description of the Advanced Research WRF Version 3, NCAR Tech. Note, NCAR/TN-475+STR, National Center for Atmospheric Research, Boulder, 105 pp.
- Stauffer, D. R., and N. L. Seaman, 1990: Use of four-dimensional data assimilation in a limited-area mesoscale model. Part I: Experiments with synoptic-scale data. *Mon. Wea. Rev.*, **118**, 1250–1277, doi: [10.1175/1520-0493\(1990\)118<1250:UOF-DDA>2.0.CO;2](https://doi.org/10.1175/1520-0493(1990)118<1250:UOF-DDA>2.0.CO;2).
- Stauffer, D. R., and N. L. Seaman, 1994: Multiscale four-dimensional data assimilation. *J. Appl. Meteor. Climatol.*, **33**, 416–434, doi: [10.1175/1520-0450\(1994\)033<0416:MFDDA>2.0.CO;2](https://doi.org/10.1175/1520-0450(1994)033<0416:MFDDA>2.0.CO;2).
- Tang, J. P., S. Y. Wang, X. R. Niu, et al., 2017: Impact of spectral nudging on regional climate simulation over CORDEX East Asia using WRF. *Climate Dyn.*, **48**, 2339–2357, doi: [10.1007/s00382-016-3208-2](https://doi.org/10.1007/s00382-016-3208-2).
- Thenkabail, P., J. W. Knox, M. Ozdogan, et al., 2012: Assessing future risks to agricultural productivity, water resources and food security: How can remote sensing help? *Photogramm. Eng. Remote Sensing*, **78**, 773–782.
- Von Storch, H., H. Langenberg, and F. Feser, 2000: A spectral nudging technique for dynamical downscaling purposes. *Mon. Wea. Rev.*, **128**, 3664–3673, doi: [10.1175/1520-0493\(2000\)128<3664:asntfd>2.0.co;2](https://doi.org/10.1175/1520-0493(2000)128<3664:asntfd>2.0.co;2).
- Xiao, C., P. L. Wu, L. X. Zhang, et al., 2016: Robust increase in extreme summer rainfall intensity during the past four decades observed in China. *Sci. Rep.*, **6**, 38506, doi: [10.1038/srep38506](https://doi.org/10.1038/srep38506).
- Ye, D. Z., Z. W. Yan, X. G. Dai, et al., 2006: A discussion of future system of weather and climate prediction. *Meteor. Mon.*, **32**, 3–8, doi: [10.3969/j.issn.1000-0526.2006.04.001](https://doi.org/10.3969/j.issn.1000-0526.2006.04.001). (in Chinese)
- Zhang, C. L., S. G. Miao, Q. C. Li, et al., 2007: Impacts of fine-resolution land use information of Beijing on a summer severe rainfall simulation. *Chinese J. Geophys.*, **50**, 1373–1382, doi: [10.3321/j.issn:0001-5733.2007.05.012](https://doi.org/10.3321/j.issn:0001-5733.2007.05.012). (in Chinese)
- Zhang, J., L. X. Peng, and P. J. Shi, 2017: Numerical simulation and diagnostic analysis on a rainstorm in Beijing 7•21 rainfall case. *J. Catastrophol.*, **32**, 191–196, 215, doi: [10.3969/j.issn.1000-811X.2017.03.032](https://doi.org/10.3969/j.issn.1000-811X.2017.03.032). (in Chinese)
- Zheng, Y. J., S. H. Liu, P. He, et al., 2017: Numerical simulation of impact of urbanization on a precipitation process: A case study of heavy rainfall in Kunming. *Acta Sci. Nat. Univ. Pekinensis*, **53**, 627–638, doi: [10.13209/j.0479-8023.2016.128](https://doi.org/10.13209/j.0479-8023.2016.128).
- Zheng, Z. F., 2013: Numerical simulation of urban effects during the “7.21” heavy rainstorm in Beijing. Proceedings of the Chinese Meteorological Society, The Eighth National Symposium on Dynamic Meteorology, Chinese Meteorological Society, Datong, Shanxi, China, 498–506.